Jurnal Pendidikan Teknik Mesin Vol 26, No. 01, June 2026 (80-96)
http://journal.unnes.ac.id

# COMPARATIVE BIOMECHANICAL ANALYSIS OF POSTERIOR MANDIBULAR PREMOLAR IMPLANTS: EFFECTS OF MATERIAL MODELING, CONTACT CONDITIONS, AND LOADING DIRECTION

**Dennis Andhara Putra[1], Kriswanto[2], Khoirul Huda[3], Jamari[4], Athanasius Priharyoto Bayuseno[5], Dhiaulhaque[6], Nurul Fatulloh[7], Mohd Syahmi Jamaludin[8]**

[1]Department of Mechanical Engineering Education, Universitas Negeri Semarang, Semarang, Central Java, Indonesia.
[2]Department of Mechanical Engineering, Universitas Diponegoro, Semarang, Central Java, Indonesia.
[3]Department of Mechanical and Manufacturing Engineering, Universiti Malaysia Sarawak, Samarahan, Sarawak, Malaysia.
Email: dens0@students.unnes.ac.id

**ABSTRACT**

Posterior tooth loss in the mandibular region may reduce masticatory performance and compromise biomechanical stability, thereby requiring predictable and well-designed implant rehabilitation strategies. This study evaluates the mechanical behavior of an implant–bone system by considering variations in bone material representation (isotropic and orthotropic models), implant–bone interface conditions (fully bonded and frictional contact), and loading orientations (axial and oblique) through a validated three-dimensional finite element analysis (3D-FEA) framework. A full factorial design comprising eight simulation configurations was implemented to assess 15 biomechanical output parameters, including von Mises stress, principal strain, and displacement across implant components and surrounding cortical and cancellous bone tissues. The results indicate that the biomechanical response of the system is strongly dependent on both structural components and loading context. The orthotropic bone model tends to increase stress and deformation responses under specific conditions, whereas oblique loading generally produces higher peak mechanical responses than axial loading. Furthermore, the influence of contact conditions is not uniform but varies according to material assumptions and loading direction, suggesting that simplified fully bonded interfaces may not fully capture realistic implant–bone interactions. Overall, the findings highlight the importance of incorporating anisotropic bone behavior, realistic interface modeling, and clinically relevant loading directions to improve the accuracy of stress prediction around dental implants. This study provides numerical evidence that may support improved implant design strategies and enhance the reliability of future finite element–based biomechanical investigations.

**Keywords:** implant biomechanical response, bone–implant mechanical behavior, computational implant modeling, orthotropic bone model, loading direction.

## INTRODUCTION

Tooth loss in the posterior mandibular region is a common clinical condition that can lead to reduced masticatory efficiency and compromised stability (Kriswanto et al., 2026; Nakamura et al., 2025). Dental implants have become a widely used restorative treatment for replacing posterior teeth because they can restore the biomechanical function of the stomatognathic system through stable osseointegration between the implant and the alveolar bone (Yorioka et al., 2024). However, the long-term success of implant therapy is greatly influenced by the biomechanical conditions within the implant–bone system during masticatory loading, particularly in the posterior region, which bears the greatest occlusal forces in the human masticatory system (Lin & Su, 2020).

The mechanical characteristics of the mandibular bone are a key factor influencing the load-transfer pattern from the implant to the peri-implant tissues. The mandibular bone consists of dense cortical and trabecular (cancellous) bone, which have different mechanical properties. These differences result in heterogeneous stress responses in both tissues when the implant is subjected to functional loads, leading to increased stress concentrations that can trigger adverse remodeling or marginal resorption in the peri-implant region (Di Stefano et al., 2021; Hosseini-faradonbeh & Katoozian, 2022; Park et al., 2022). Understanding the distribution of stress in the cortical and cancellous bone around the implant is crucial for minimizing the risk of biomechanical failure and maintaining the long-term integrity of the peri-implant bone. However, the complex interaction between bone and implants makes direct experimental assessment difficult (Hosseini-faradonbeh & Katoozian, 2022; Qiu et al., 2024).

Numerical methods such as Finite Element Analysis (FEA) have emerged as reliable tools for predicting the biomechanical response of the implant–bone system before clinical application. FEA simulations enable the evaluation of complex variables, including the anisotropic properties of bone tissue, contact interactions between implant components and bone, and variations in the direction and magnitude of functional loads—factors that are difficult to measure empirically in humans. Furthermore, FEA models can more realistically represent the material properties of cortical and cancellous bone, thereby aiding in the understanding of stress distribution around the implant and supporting design optimization and clinical strategies to enhance the long-term stability of dental implants (Hosseini-faradonbeh & Katoozian, 2022; Prados-privado et al., n.d.).

Although Finite Element Analysis (FEA) has been used to evaluate the biomechanical behavior of dental implant systems and peri-implant bone tissue, most numerical studies still assume bone material is isotropic, even though cortical and trabecular bone are biologically and mechanically anisotropic/orthotropic. Various studies indicate that isotropic models still dominate FEA research due to their ease of numerical implementation, while studies directly comparing the effects of isotropic and orthotropic models on stress and strain distributions around the implant remain limited. These differences in material definition can affect the accuracy of biomechanical predictions, particularly in peri-implant bone tissue that undergoes complex load transfer (Prados-Privado et al., 2020; Taheri et al., 2018).

Most FEA studies on dental implants assume fully bonded contact conditions at the implant–bone interface to represent perfect osseointegration. This approach does not fully represent actual clinical conditions, as the interaction between the implant and bone may also involve frictional contact. Although some studies have evaluated the influence of contact conditions on stress distribution, comprehensive analyses combining variations in bonded and frictional contact conditions with different bone material models are still rarely performed within a single integrated simulation framework. In fact, these contact characteristics directly influence the distribution of stress, strain, and displacement in cortical and cancellous bone, as well as in the implant system components (Dhatrak et al., 2023).

On the other hand, the direction of functional loading also plays a significant role in the biomechanical response of the implant system. Oblique loading has been reported to produce higher stress concentrations than axial loading due to the presence of lateral forces and bending moments in the implant structure and its supporting tissues. However, most previous studies have been limited to partial evaluations, focusing either solely on bone tissue or on specific implant components. Systematic comparisons of the effects of axial and oblique loading on multi-parameter biomechanical responses—including stress, strain, and displacement in the fixture, screw, abutment, and peri-implant bone tissue—under various combinations of material and contact conditions have not yet been widely reported (Azhdari et al., 2026; Falcinelli et al., 2023).

Most studies treat bone material modeling, interface conditions, or load direction as independent factors. However, such a separate approach risks overlooking the interaction effects between the orthotropic behavior of bone, implant-bone contact mechanics, and non-axial loads, resulting in incomplete predictions of the stress-strain-displacement response in both the implant component and the surrounding bone (Falcinelli et al., 2023).

Therefore, this study aims to evaluate the simultaneous effects of the material properties of the posterior mandibular bone (orthotropic and isotropic), implant–bone contact conditions (fully bonded and frictional contact), and loading direction (axial and oblique) on the biomechanical response of the dental implant system using three-dimensional finite element analysis simulations. The evaluation was conducted on 15 biomechanical parameters, including the distribution of stress, strain, and displacement in the implant and cortical-cancellous bone components. This study is expected to provide a more realistic understanding of the biomechanical behavior of dental implants and improve the accuracy of numerical modeling in dental implantology FEA studies.

## METHODS

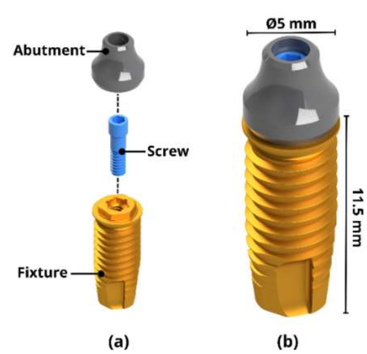


Figure 1. Components and assembly of the dental implant system: (a) Exploded view showing the abutment, screw, and fixture; (b) Assembled implant illustrating the final configuration.

A three-dimensional model of a dental implant system was developed to simulate the biomechanical response of a single implant in the posterior region of the lower first premolar using the finite element analysis (FEA) approach, as shown in Figure 1. The model consists of five main components: the fixture, the abutment, the screw, the cortical bone, and the cancellous bone. The model consists of five main components: the fixture, abutment, screw, cortical bone, and cancellous bone. Each component is modeled as a separate solid domain, allowing mechanical interactions between structures to be explicitly defined during the numerical analysis.

The implant geometry, which includes the fixture, abutment, and screw, was designed using Autodesk Inventor Professional 2025 computer-aided design (CAD) software based on clinical implant dimensions suitable for single-tooth rehabilitation in the mandibular posterior region. The fixture has a diameter of 5 mm, a length of 11.5 mm, a pitch of 0.8 mm, a thread height of 0.4 mm, and a V-shaped thread profile. Key geometric features, including the shape of the implant body and the fixture threads, are retained in the model to represent the mechanical characteristics relevant to load transfer from the prosthetic components to the peri-implant bone tissue.

The mandibular bone model is represented as a posterior alveolar bone segment, consisting of two tissue domains: cortical bone, the denser outer layer, and cancellous bone, the internal trabecular tissue. These two domains were separated so that the material properties of each tissue could be defined independently based on its biomechanical characteristics. The implant was positioned vertically in the first mandibular premolar region as a clinically relevant single-implant rehabilitation scenario. Figure 2 illustrates the reconstructed implant–bone geometry, showing the separation of cortical and cancellous bone domains used for independent material assignment in the FEA model. The mandibular bone geometry was developed as a solid bone block using CAD software, with a height of 15 mm, a width of 20 mm, and a cortical layer thickness of 0.5 mm, followed by Boolean segmentation into cortical and cancellous regions to represent anisotropic bone characteristics. (Alqahtani et al., 2023). The final model was exported to the ANSYS Workbench 2023 R1 FEA software in IGES format for further numerical analysis.

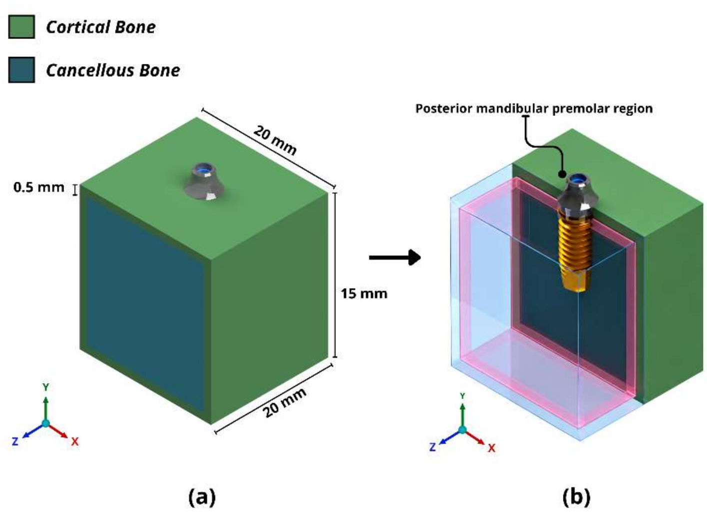


Figure 2. 3D geometric reconstruction of the implant–bone model. (a) Structural configuration of cortical and cancellous bone domains. (b) Sectional visualization of the dental implant positioned within the bone block.

Based on the three-dimensional model developed, the simulation was designed to evaluate the effects of bone material properties, implant–bone contact conditions, and loading direction on the biomechanical response of the implant–bone system. These three factors were varied in a full 2 × 2 × 2 factorial design, with isotropic/orthotropic materials, fully bonded/frictional contact, and axial/oblique loading, yielding eight simulation scenarios. In each scenario, fifteen biomechanical outputs were evaluated, including stress, strain, and displacement in the implant components and peri-implant bone. Comparisons between scenarios were performed to assess changes in biomechanical response and the sensitivity of each parameter. The simulation combination matrix is presented in Table 1.

Table 1. The matrix of bone material properties, implant-bone contact, and loading direction used in the FEA analysis

| Run | Bone material | Implant-bone contact | Loading direction |
|---|---|---|---|
| 1 | Isotropic | Fully bonded | Axial |
| 2 | Isotropic | Fully bonded | Oblique |
| 3 | Isotropic | Frictional contact | Axial |
| 4 | Isotropic | Frictional contact | Oblique |
| 5 | Orthotropic | Fully bonded | Axial |
| 6 | Orthotropic | Fully bonded | Oblique |
| 7 | Orthotropic | Frictional contact | Axial |
| 8 | Orthotropic | Frictional contact | Oblique |

Note: *The design matrix represents the full factorial combination of two bone material definitions, two implant-bone contact conditions, and two loading directions.*

The material properties of all components in the 3D model were determined based on the latest biomechanical literature and applied in a Static Structural finite element analysis (FEA) simulation. The mandibular bone was analyzed using both orthotropic and isotropic material approaches. At the same time, the components of the implant system—including the fixture, abutment, and screw—were modeled as isotropic Ti-6Al-4V titanium alloy. The detailed values of Young's modulus, shear modulus, and Poisson's ratio for each material are presented in Table 2.

Table 2. Material Properties.

| Material / Component | Young's Modulus (GPa) | Shear Modulus (GPa) | Poisson Ratio (ν) | Reference |
|---|---|---|---|---|
| Implant system | 113.8 | - | 0.342 | (MatWeb, 2026) |
| Cortical Bone (Isotropic) | 13.7 | 5.27 | 0.30 | (Le et al., 2016) |
| Cancellous Bone (Isotropic) | 1.37 | 0.53 | 0.30 | (Le et al., 2016) |
| Cortical Bone (Orthotropic) | $E_x$=12.7, $E_y$=22.8, $E_z$=17.9 | $G_{xy}$=5.5, $G_{yz}$=7.4, $G_{xz}$=5.0 | $\nu_{xy}$=0.31, $\nu_{yz}$=0, $\nu_{xz}$=0.18 | (Ding et al., 2014) |
| Cancellous Bone (Orthotropic) | $E_x$=0.551, $E_y$=0.907, $E_z$=0.114 | $G_{xy}$=0.434, $G_{yz}$=0.81, $G_{xz}$=0.078 | $\nu_{xy}$=0.31, $\nu_{yz}$=0, $\nu_{xz}$=0.22 | (Ding et al., 2014) |

In finite element analysis (FEA) simulations of dental implants, the contact interface between the implant and the bone determines the load transfer mechanism as well as the distribution of stress, strain, and micromotion. This interface is generally modeled as fully bonded or frictional contact, depending on the assumed degree of osseointegration. (Dhatrak et al., 2023). In fully bonded contact, the surfaces of the implant and bone are assumed to be perfectly bonded, without slip, mimicking complete osseointegration in which loads are transmitted directly without tangential friction; Thus, it is often used as a reference condition for assessing interface stability after biological and mechanical integration. (Han et al., 2016). In contrast, frictional contact involves partial interface contact, such as during the early stages of osseointegration or immediate loading, where normal contact is maintained, and the coefficient of friction controls the tangential response. (Niroomand & Arabbeiki, 2020). Contact interactions in the FEA model are applied at the interfaces between the implant and bone, namely: (i) the abutment with cortical bone, (ii) the fixture with cortical bone

and (iii) the fixture with cancellous bone, with μ = 0.38 in accordance with parameters from previous numerical and experimental studies, allowing the interfaces to undergo limited micromotion during loading (Fodor & Pałka, 2025). This approach to the two contact conditions allows a comparative evaluation of full and partial osseointegration, providing a systematic biomechanical framework for assessing stress concentrations, strains, micromotion, and the mechanical stability of the implant–bone system. (Niroomand & Arabbeiki, 2020).

The load was applied to the abutment surface, as reported in the literature, to simulate clinical conditions in the posterior premolar region. As shown in Figure 3, an axial load was applied parallel to the implant long axis with a vertical component of 140 N, assumed as the physiological bite force in the first premolar region, and a tangential component of 16.45 N. Meanwhile, an oblique load was applied with a vertical component of 100 N at a 30° angle to the implant long axis, representing lateral forces during unilateral mastication. The load application point was located at the apex of the abutment to simulate physiological force distribution on the prosthesis. Fixed support was applied at the mesial and distal cut surfaces of the bone block, including cortical and cancellous bone, to restrict translation and represent the mechanical constraint of the surrounding mandibular bone segments. The oblique force components (Fx, Fy, Fz) were calculated via vector decomposition for stress and micromotion analysis (Kamal et al., 2025; Luo et al., 2022).

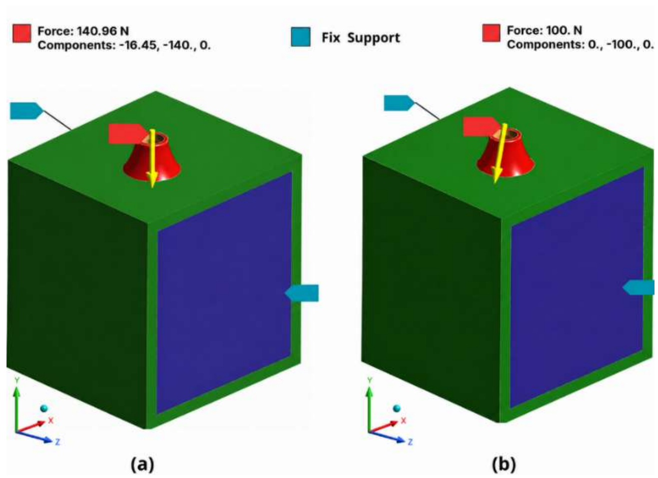

Figure 3. Loading directions and fixed support. (a) Oblique load. (b) Axial load.

The loads are static and linear, applied to evaluate the distribution of stress and strain throughout the implant structure and the peri-implant bone, assuming linear-elastic materials. At the frictional interface, contact behavior is calculated nonlinearly, ensuring numerical consistency without dynamic inertial effects. The lateral and basal surfaces of the mandible are constrained against translation to simulate simplified clinical fixation conditions, consistent with standard FEA methodology in dental implant studies (Has, 2025).

The mesh was discretized using quadratic tetrahedral elements, with local mesh refinement at the implant-bone interface to improve stress distribution accuracy in critical areas (Alemayehu & Todoh, 2024). The local element size is set to 0.5 mm in cortical bone and 0.6 mm in cancellous bone, with a global mesh size of 4.7 mm. Convergence is evaluated based on changes in von Mises stress at the fixture, screw, and abutment, as well as the maximum principal stress in cortical and cancellous bone, using a criterion of <5% change between refinement levels to ensure numerical stability. A summary of the convergence test results is shown in Table 3. The results include the distributions of stress, strain, and micromotion throughout the implant-bone complex, analyzed under linear-elastic and static conditions.

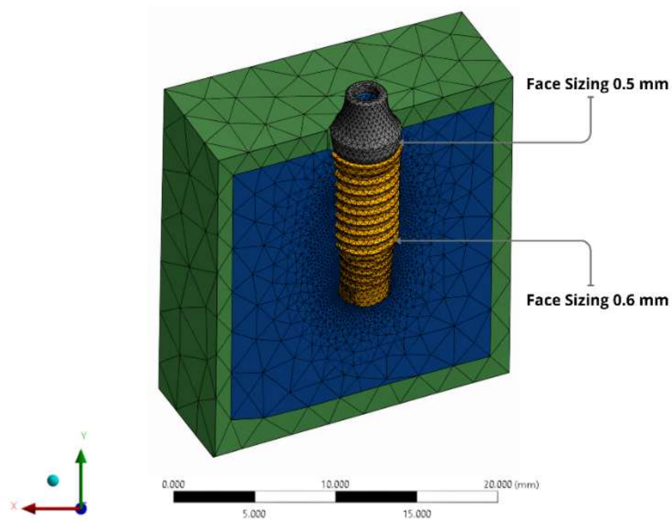


Figure 4. Finite element mesh configuration of the implant–bone model employing quadratic tetrahedral elements.

Table 3. Mesh Convergence Analysis of Global Element Size on von Mises Stress and Strain

| Global Element Size (mm) | $\sigma_{von}$F (MPa) | $\sigma_{von}$S (MPa) | $\sigma_{von}$A (MPa) | σCt (MPa) | σCn (MPa) |
|---|---|---|---|---|---|
| 4.8 | 45.8 | 154.97 | 96.32 | 0.234 | 6.312 |
| 4.7 | 45.8 | 154.89 | 96.16 | 0.238 | 6.312 |
| 4.6 | 45.8 | 154.95 | 96.2 | 0.246 | 6.335 |
| Variation 4.8:4.7 (%) | 0.00 | 0.06 | -0.16 | -1.70 | 0.00 |
| Variation 4.7:4.6 (%) | 0.00 | -0.04 | -0.04 | -3.47 | 0.37 |

To verify the reliability of the finite element model, the von Mises stress results were systematically compared with a previously published dental implant simulation by Talmazov et al., which used Y-TZP zirconia and a load of 178 N. The observed deviation of 0.9% indicates excellent agreement between the two models. This close agreement confirms that the current FEA model is robust and sufficiently accurate to support further biomechanical analysis of stress distribution in dental implant structures (Kriswanto, Bayuseno et al., 2025).

The numerical analysis focused on 15 biomechanical parameters representing the distribution of stress, strain, and displacement in the implant–bone system. The parameters evaluated included von Mises stress and von Mises strain in each implant component (fixture, abutment, and screw), as well as principal stress and principal strain in the cortical and cancellous bone. Additionally, displacements in each implant component and bone tissue were extracted to evaluate global deformation and peri-implant micromotion. All parameters were selected as key biomechanical indicators to quantify the influence of material properties, contact conditions, and loading direction on the structural stability of the implant–bone system. All outputs were then analyzed across scenarios to assess model consistency and the sensitivity of biomechanical responses to parameter variations within a validated finite-element analysis framework.

Data analysis was performed by comparing biomechanical responses across scenarios that included variations in bone material properties, implant–bone contact conditions, and loading directions. Each output was evaluated to identify the effects of orthotropic and isotropic material assumptions, bonded and frictional contact conditions, and axial and oblique loading configurations on the distribution of stress, strain, and displacement in the implant–bone system. Quantitative response changes were calculated using percentage delta (%) for each output variable to assess biomechanical sensitivity to each simulation parameter.

The results are then systematically presented based on output categories, including stress, strain, and displacement, to facilitate direct comparisons between scenarios. This approach enables a structured evaluation of the interactions among key biomechanical factors. It enhances the reliability of numerical interpretations within a validated finite element analysis (FEA) framework for dental implants (Qiu et al., 2024).

## RESULTS AND DISCUSSION

Results of biomechanical simulations of the implant–bone system for eight model configurations are shown in Figures 6–8. These configurations represent combinations of two bone material assumptions (isotropic and orthotropic), two contact conditions (bonded and frictional), and two loading directions (axial and oblique). The output parameters analyzed include Von Mises stress and strain at the fixture, screw, and abutment; maximum principal stress and strain in cortical and cancellous bone; and displacement in each implant component and bone tissue.

In general, the simulation results show that the biomechanical response does not follow a single pattern but varies with component type, bone tissue type, contact conditions, and loading direction. Changing the material model from isotropic to orthotropic yields non-uniform responses across all parameters. In some configurations, the orthotropic model produces higher stress or displacement in certain components, whereas in others it yields lower values than the isotropic model. This indicates that the influence of bone material definition is specific to the observed biomechanical outputs.

The highest von Mises stress value in the implant components was found in the fixture, at 503.12 MPa, in the isotropic–frictional–oblique configuration. Meanwhile, the highest maximum principal stress in cortical bone was recorded at 18.065 MPa in the orthotropic–bonded–axial configuration, while the highest value in cancellous bone reached 88.099 MPa in the isotropic–bonded–oblique configuration. These findings indicate that the locations of maximum stress differ between the implant component and the bone tissue, so the biomechanical response cannot be generalized from a single simulation configuration.

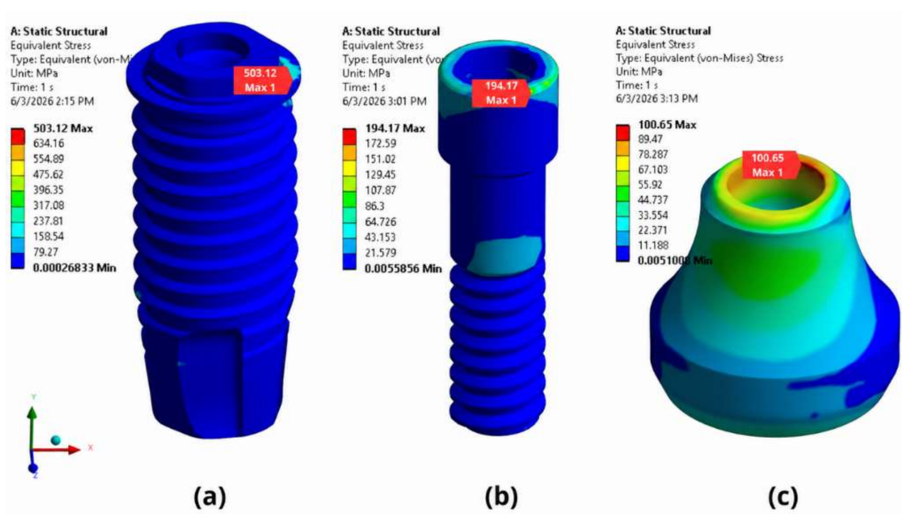


Figure 5. Maximum von Mises stress distribution in implant components: (a) fixture, (b) abutment screw, and (c) abutment. The contour plots show the location of peak equivalent stress in each component, with stress values reported in MPa.

Based on the displacement parameter, the maximum value was found in the cancellous bone at 27.59 μm in the orthotropic–bonded–oblique configuration. The same configuration also produced the highest displacements in the fixture, screw, abutment, and cortical bone, at 15.59 μm, 15.72 μm, 16.33 μm, and 13.99 μm, respectively. This pattern indicates that the combination of orthotropic material, bonded contact, and oblique loading produces the greatest displacement response in all analyzed components.

A comparison between bonded and frictional contact conditions shows that the contact effect depends on the material combination and loading direction. Under certain axial loading conditions, frictional contact results in higher stress and displacement than bonded contact, particularly in implant components. However, in certain configurations involving orthotropic materials and oblique loading, frictional contact does not always increase biomechanical response. Therefore, the influence of contact conditions must be evaluated specifically for each output parameter.

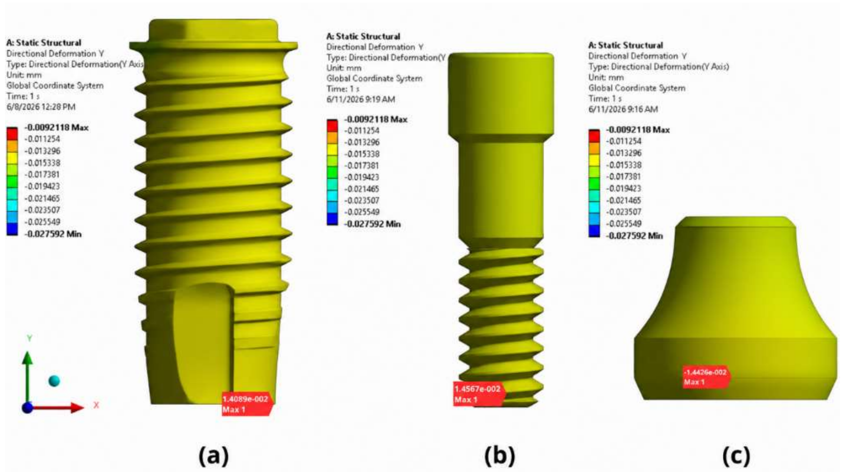


Figure 6. The figure shows the highest directional deformation along the Y-axis for each implant component: (a) fixture, (b) screw, and (c) abutment. Values are extracted from FEA simulation to highlight peak displacement regions.

The loading direction also clearly affects the distribution of stress, strain, and displacement. Oblique loading tends to produce higher biomechanical responses in several parameters, particularly at the fixture and in cancellous bone, compared to axial loading. However, this pattern is not consistent across all material and contact combinations. Therefore, these results emphasize that biomechanical evaluation of the implant–bone system must simultaneously consider the interactions between bone material, contact conditions, and loading direction. A safety factor (FoS) of approximately 1.75 under the most critical conditions indicates that the implant structure remains mechanically safe (FoS > 1), even though the oblique loading configuration with frictional contact produces the highest stress.

Table 4. Effect of bone material modeling on biomechanical outputs.

| Biomechanical output | Load | Contact | Isotropic | Orthotropic | Δ (%) |
|---|---|---|---|---|---|
| σvonF (MPa) | Axial | Bonded | 45.8 | 54.084 | 18.09% |
| σvonS (MPa) | Axial | Bonded | 154.89 | 153.51 | -0.89% |
| σvonA (MPa) | Axial | Bonded | 96.166 | 96.192 | 0.03% |
| σCt (MPa) | Axial | Bonded | 0.23804 | 18.065 | 7489.06% |
| σCn (MPa) | Axial | Bonded | 6.3122 | 3.393 | -46.25% |
| εF (-) | Axial | Bonded | 4.87E-04 | 5.27E-04 | 8.21% |
| εS (-) | Axial | Bonded | 1.31E-03 | 1.30E-03 | -0.89% |
| εA (-) | Axial | Bonded | 8.13E-04 | 8.13E-04 | 0.03% |
| εCt (-) | Axial | Bonded | 3.60E-04 | 9.65E-04 | 168.06% |
| εCn (-) | Axial | Bonded | 4.06E-04 | 5.68E-03 | 1299.61% |
| δF (μm) | Axial | Bonded | 1.07 | 0.67 | -37.38% |
| δS (μm) | Axial | Bonded | 1.46 | 1.48 | 1.37% |
| δA (μm) | Axial | Bonded | 1.87 | 2.01 | 7.49% |
| δCt (μm) | Axial | Bonded | 1.26 | 1.48 | 17.46% |
| δCn (μm) | Axial | Bonded | 1.08 | 1.48 | 37.04% |
| σvonF (MPa) | Axial | Frictional | 76.161 | 81.312 | 6.76% |
| σvonS (MPa) | Axial | Frictional | 171.92 | 194.17 | 12.94% |

| Biomechanical output | Load | Contact | Isotropic | Orthotropic | Δ (%) |
|---|---|---|---|---|---|
| σvonA (MPa) | Axial | Frictional | 96.025 | 96.271 | 0.26% |
| σCt (MPa) | Axial | Frictional | 3.2586 | 12.607 | 286.88% |
| σCn (MPa) | Axial | Frictional | 9.7093 | 2.1367 | -77.99% |
| εF (-) | Axial | Frictional | 7.33E-04 | 7.59E-04 | 3.53% |
| εS (-) | Axial | Frictional | 1.51E-03 | 7.59E-04 | -49.74% |
| εA (-) | Axial | Frictional | 8.13E-04 | 8.15E-04 | 0.25% |
| εCt (-) | Axial | Frictional | 1.83E-03 | 6.80E-04 | -62.96% |
| εCn (-) | Axial | Frictional | 5.60E-04 | 3.05E-03 | 445.64% |
| δF (μm) | Axial | Frictional | 1.18 | 1.91 | 61.86% |
| δS (μm) | Axial | Frictional | 2.97 | 4.24 | 42.76% |
| δA (μm) | Axial | Frictional | 4.29 | 5.67 | 32.17% |
| δCt (μm) | Axial | Frictional | 1.53 | 2.31 | 50.98% |
| δCn (μm) | Axial | Frictional | 1.21 | 2.01 | 66.12% |
| σvonF (MPa) | Oblique | Bonded | 457.05 | 43.358 | -90.51% |
| σvonS (MPa) | Oblique | Bonded | 39.267 | 36.92 | -5.98% |
| σvonA (MPa) | Oblique | Bonded | 96.025 | 98.037 | 2.10% |
| σCt (MPa) | Oblique | Bonded | 0.94895 | 16.364 | 1624.43% |
| σCn (MPa) | Oblique | Bonded | 88.099 | 6.9625 | -92.10% |
| εF (-) | Oblique | Bonded | 5.13E-03 | 3.65E-04 | -92.89% |
| εS (-) | Oblique | Bonded | 3.43E-04 | 3.28E-04 | -4.38% |
| εA (-) | Oblique | Bonded | 8.28E-04 | 8.29E-04 | 0.11% |
| εCt (-) | Oblique | Bonded | 7.08E-04 | 9.38E-04 | 32.56% |
| εCn (-) | Oblique | Bonded | 9.55E-03 | 1.39E-02 | 45.81% |
| δF (μm) | Oblique | Bonded | 5.51 | 15.59 | 182.94% |
| δS (μm) | Oblique | Bonded | 5.2 | 15.72 | 202.31% |
| δA (μm) | Oblique | Bonded | 6.25 | 16.33 | 161.28% |
| δCt (μm) | Oblique | Bonded | 3.06 | 13.99 | 357.19% |
| δCn (μm) | Oblique | Bonded | 21.65 | 27.59 | 27.44% |
| σvonF (MPa) | Oblique | Frictional | 503.12 | 53.443 | -89.38% |
| σvonS (MPa) | Oblique | Frictional | 46.189 | 36.839 | -20.24% |
| σvonA (MPa) | Oblique | Frictional | 97.947 | 100.65 | 2.76% |
| σCt (MPa) | Oblique | Frictional | 0.28687 | 4.4476 | 1450.39% |
| σCn (MPa) | Oblique | Frictional | 82.938 | 7.4902 | -90.97% |
| εF (-) | Oblique | Frictional | 5.50E-03 | 4.83E-04 | -91.22% |
| εS (-) | Oblique | Frictional | 4.04E-04 | 3.19E-04 | -21.15% |
| εA (-) | Oblique | Frictional | 8.82E-04 | 8.52E-04 | -3.37% |
| εCt (-) | Oblique | Frictional | 2.46E-04 | 3.12E-04 | 26.89% |
| εCn (-) | Oblique | Frictional | 9.67E-03 | 3.62E-04 | -96.26% |
| δF (μm) | Oblique | Frictional | 4.01 | 1.21 | -69.83% |
| δS (μm) | Oblique | Frictional | 4.01 | 3.79 | -5.49% |
| δA (μm) | Oblique | Frictional | 3.35 | 5.51 | 64.48% |
| δCt (μm) | Oblique | Frictional | 0.86 | 1.62 | 88.37% |
| δCn (μm) | Oblique | Frictional | 22.88 | 0.89 | -96.11% |

Table 5. Effect of implant-bone contact condition on biomechanical outputs.

| Biomechanical output | Material | Load | Bonded | Friction | Δ (%) |
|---|---|---|---|---|---|
| σvonF (MPa) | Isotropic | Axial | 45.80 | 76.16 | 66.3% |
| σvonS (MPa) | Isotropic | Axial | 154.89 | 171.92 | 11.0% |
| σvonA (MPa) | Isotropic | Axial | 96.17 | 96.03 | -0.1% |
| σCt (MPa) | Isotropic | Axial | 0.24 | 3.26 | 1268.9% |
| σCn (MPa) | Isotropic | Axial | 6.31 | 9.71 | 53.8% |
| εF (-) | Isotropic | Axial | 4.87E-04 | 7.33E-04 | 50.6% |
| εS (-) | Isotropic | Axial | 1.31E-03 | 1.51E-03 | 15.3% |
| εA (-) | Isotropic | Axial | 8.13E-04 | 8.13E-04 | 0.1% |
| εCt (-) | Isotropic | Axial | 3.60E-04 | 1.83E-03 | 409.8% |
| εCn (-) | Isotropic | Axial | 4.06E-04 | 5.60E-04 | 37.9% |
| δF (μm) | Isotropic | Axial | 1.07 | 1.18 | 10.3% |
| δS (μm) | Isotropic | Axial | 1.46 | 2.97 | 103.4% |
| δA (μm) | Isotropic | Axial | 1.87 | 4.29 | 129.4% |
| δCt (μm) | Isotropic | Axial | 1.26 | 1.53 | 21.4% |
| δCn (μm) | Isotropic | Axial | 1.08 | 1.21 | 12.0% |
| σvonF (MPa) | Orthotropic | Axial | 54.084 | 81.312 | 50.3% |
| σvonS (MPa) | Orthotropic | Axial | 153.51 | 194.17 | 26.5% |
| σvonA (MPa) | Orthotropic | Axial | 96.192 | 96.271 | 0.1% |
| σCt (MPa) | Orthotropic | Axial | 18.065 | 12.607 | -30.2% |
| σCn (MPa) | Orthotropic | Axial | 3.393 | 2.1367 | -37.0% |
| εF (-) | Orthotropic | Axial | 5.27E-04 | 7.59E-04 | 44.1% |
| εS (-) | Orthotropic | Axial | 1.30E-03 | 7.59E-04 | -41.5% |
| εA (-) | Orthotropic | Axial | 8.13E-04 | 8.15E-04 | 0.3% |
| εCt (-) | Orthotropic | Axial | 9.65E-04 | 6.80E-04 | -29.6% |
| εCn (-) | Orthotropic | Axial | 5.68E-03 | 3.05E-03 | -46.2% |
| δF (μm) | Orthotropic | Axial | 0.67 | 1.91 | 185.1% |
| δS (μm) | Orthotropic | Axial | 1.48 | 4.24 | 186.5% |
| δA (μm) | Orthotropic | Axial | 2.01 | 5.67 | 182.1% |
| δCt (μm) | Orthotropic | Axial | 1.48 | 2.31 | 56.1% |
| δCn (μm) | Orthotropic | Axial | 1.48 | 2.01 | 35.8% |
| σvonF (MPa) | Isotropic | Oblique | 457.05 | 503.12 | 10.1% |
| σvonS (MPa) | Isotropic | Oblique | 39.27 | 46.189 | 17.6% |
| σvonA (MPa) | Isotropic | Oblique | 96.03 | 97.947 | 2.0% |
| σCt (MPa) | Isotropic | Oblique | 0.949 | 0.287 | -69.8% |
| σCn (MPa) | Isotropic | Oblique | 88.099 | 82.938 | -5.9% |
| εF (-) | Isotropic | Oblique | 5.13E-03 | 5.50E-03 | 7.0% |
| εS (-) | Isotropic | Oblique | 3.43E-04 | 4.04E-04 | 18.1% |
| εA (-) | Isotropic | Oblique | 8.28E-04 | 8.82E-04 | 6.6% |
| εCt (-) | Isotropic | Oblique | 7.08E-04 | 2.46E-04 | -65.3% |
| εCn (-) | Isotropic | Oblique | 9.55E-03 | 9.67E-03 | 1.3% |
| δF (μm) | Isotropic | Oblique | 5.51 | 4.01 | -27.2% |
| δS (μm) | Isotropic | Oblique | 5.2 | 4.01 | -22.9% |
| δA (μm) | Isotropic | Oblique | 6.25 | 3.35 | -46.4% |
| δCt (μm) | Isotropic | Oblique | 3.06 | 0.86 | -71.9% |
| δCn (μm) | Isotropic | Oblique | 21.65 | 22.88 | 5.7% |
| σvonF (MPa) | Orthotropic | Oblique | 43.358 | 53.443 | 23.3% |
| σvonS (MPa) | Orthotropic | Oblique | 36.92 | 36.839 | -0.2% |
| σvonA (MPa) | Orthotropic | Oblique | 98.037 | 100.65 | 2.7% |

| Biomechanical output | Material | Load | Bonded | Friction | Δ (%) |
|---|---|---|---|---|---|
| σCt (MPa) | Orthotropic | Oblique | 16.364 | 4.4476 | -72.8% |
| σCn (MPa) | Orthotropic | Oblique | 6.9625 | 7.4902 | 7.6% |
| εF (-) | Orthotropic | Oblique | 3.65E-04 | 4.83E-04 | 32.2% |
| εS (-) | Orthotropic | Oblique | 3.28E-04 | 3.19E-04 | -2.6% |
| εA (-) | Orthotropic | Oblique | 8.29E-04 | 8.52E-04 | 2.9% |
| εCt (-) | Orthotropic | Oblique | 9.38E-04 | 3.12E-04 | -66.7% |
| εCn (-) | Orthotropic | Oblique | 1.39E-02 | 3.62E-04 | -97.4% |
| δF (μm) | Orthotropic | Oblique | 15.59 | 1.21 | -92.2% |
| δS (μm) | Orthotropic | Oblique | 15.72 | 3.79 | -75.9% |
| δA (μm) | Orthotropic | Oblique | 16.33 | 5.51 | -66.3% |
| δCt (μm) | Orthotropic | Oblique | 13.99 | 1.62 | -88.4% |
| δCn (μm) | Orthotropic | Oblique | 27.59 | 0.89 | -96.8% |

Table 6. Effect of loading direction on biomechanical outputs.

| Biomechanical output | Material | Contact | Axial Load | Oblique Load | Δ (%) |
|---|---|---|---|---|---|
| σvonF (MPa) | Isotropic | Bonded | 45.8 | 457.05 | 897.93% |
| σvonS (MPa) | Isotropic | Bonded | 154.89 | 39.267 | -74.65% |
| σvonA (MPa) | Isotropic | Bonded | 96.166 | 96.025 | -0.15% |
| σCt (MPa) | Isotropic | Bonded | 0.23804 | 0.94895 | 298.65% |
| σCn (MPa) | Isotropic | Bonded | 6.3122 | 88.099 | 1295.69% |
| εF (-) | Isotropic | Bonded | 4.90E-04 | 5.13E-03 | 946.94% |
| εS (-) | Isotropic | Bonded | 1.31E-03 | 3.40E-04 | -74.05% |
| εA (-) | Isotropic | Bonded | 8.10E-04 | 8.30E-04 | 2.47% |
| εCt (-) | Isotropic | Bonded | 3.60E-04 | 7.10E-04 | 97.22% |
| εCn (-) | Isotropic | Bonded | 4.10E-04 | 9.55E-03 | 2229.27% |
| δF (μm) | Isotropic | Bonded | 1.07 | 5.51 | 414.95% |
| δS (μm) | Isotropic | Bonded | 1.46 | 5.2 | 256.16% |
| δA (μm) | Isotropic | Bonded | 1.87 | 6.25 | 234.22% |
| δCt (μm) | Isotropic | Bonded | 1.26 | 3.06 | 142.86% |
| δCn (μm) | Isotropic | Bonded | 1.08 | 21.65 | 1904.63% |
| σvonF (MPa) | Isotropic | Frictional | 76.161 | 503.12 | 560.60% |
| σvonS (MPa) | Isotropic | Frictional | 171.92 | 46.189 | -73.13% |
| σvonA (MPa) | Isotropic | Frictional | 96.025 | 97.947 | 2.00% |
| σCt (MPa) | Isotropic | Frictional | 3.2586 | 0.28687 | -91.20% |
| σCn (MPa) | Isotropic | Frictional | 9.7093 | 82.938 | 754.21% |
| εF (-) | Isotropic | Frictional | 7.30E-04 | 5.50E-03 | 653.42% |
| εS (-) | Isotropic | Frictional | 1.51E-03 | 4.00E-04 | -73.51% |
| εA (-) | Isotropic | Frictional | 8.10E-04 | 8.80E-04 | 8.64% |
| εCt (-) | Isotropic | Frictional | 1.83E-03 | 2.50E-04 | -86.34% |
| εCn (-) | Isotropic | Frictional | 5.60E-04 | 9.67E-03 | 1626.79% |
| δF (μm) | Isotropic | Frictional | 1.18 | 4.01 | 239.83% |
| δS (μm) | Isotropic | Frictional | 2.97 | 4.01 | 35.02% |
| δA (μm) | Isotropic | Frictional | 4.29 | 3.35 | -21.91% |
| δCt (μm) | Isotropic | Frictional | 1.53 | 0.86 | -43.79% |
| δCn (μm) | Isotropic | Frictional | 1.21 | 22.88 | 1790.91% |
| σvonF (MPa) | Orthotropic | Bonded | 54.084 | 43.358 | -19.83% |
| σvonS (MPa) | Orthotropic | Bonded | 153.51 | 36.92 | -75.95% |
| σvonA (MPa) | Orthotropic | Bonded | 96.192 | 98.037 | 1.92% |
| σCt (MPa) | Orthotropic | Bonded | 18.065 | 16.364 | -9.42% |

| Biomechanical output | Material | Contact | Axial Load | Oblique Load | Δ (%) |
|---|---|---|---|---|---|
| σCn (MPa) | Orthotropic | Bonded | 3.393 | 6.9625 | 105.20% |
| εF (-) | Orthotropic | Bonded | 5.30E-04 | 3.70E-04 | -30.19% |
| εS (-) | Orthotropic | Bonded | 1.30E-03 | 3.30E-04 | -74.62% |
| εA (-) | Orthotropic | Bonded | 8.10E-04 | 8.30E-04 | 2.47% |
| εCt (-) | Orthotropic | Bonded | 9.60E-04 | 9.40E-04 | -2.08% |
| εCn (-) | Orthotropic | Bonded | 5.68E-03 | 1.39E-02 | 145.07% |
| δF (μm) | Orthotropic | Bonded | 0.67 | 15.59 | 2226.87% |
| δS (μm) | Orthotropic | Bonded | 1.48 | 15.72 | 962.16% |
| δA (μm) | Orthotropic | Bonded | 2.01 | 16.33 | 712.44% |
| δCt (μm) | Orthotropic | Bonded | 1.48 | 13.99 | 845.27% |
| δCn (μm) | Orthotropic | Bonded | 1.48 | 27.59 | 1764.19% |
| σvonF (MPa) | Orthotropic | Frictional | 81.312 | 53.443 | -34.27% |
| σvonS (MPa) | Orthotropic | Frictional | 194.17 | 36.839 | -81.03% |
| σvonA (MPa) | Orthotropic | Frictional | 96.271 | 100.65 | 4.55% |
| σCt (MPa) | Orthotropic | Frictional | 12.607 | 4.4476 | -64.72% |
| σCn (MPa) | Orthotropic | Frictional | 2.1367 | 7.4902 | 250.55% |
| εF (-) | Orthotropic | Frictional | 7.60E-04 | 4.80E-04 | -36.84% |
| εS (-) | Orthotropic | Frictional | 7.60E-04 | 3.20E-04 | -57.89% |
| εA (-) | Orthotropic | Frictional | 8.20E-04 | 8.50E-04 | 3.66% |
| εCt (-) | Orthotropic | Frictional | 6.80E-04 | 3.10E-04 | -54.41% |
| εCn (-) | Orthotropic | Frictional | 3.05E-03 | 3.60E-04 | -88.20% |
| δF (μm) | Orthotropic | Frictional | 1.91 | 1.21 | -36.65% |
| δS (μm) | Orthotropic | Frictional | 4.24 | 3.79 | -10.61% |
| δA (μm) | Orthotropic | Frictional | 5.67 | 5.51 | -2.82% |
| δCt (μm) | Orthotropic | Frictional | 2.31 | 1.62 | -29.87% |
| δCn (μm) | Orthotropic | Frictional | 2.01 | 0.89 | -55.72% |

Modeling bone material results in clear numerical changes in the biomechanical response of the implant–bone system, particularly in the peri-implant bone tissue. The abutment exhibits relatively small changes in stress and strain in most scenarios. In contrast, the fixture and screw continue to exhibit responses that depend on the loading direction and contact conditions. The transition from an isotropic to an orthotropic model consistently alters the distribution of stress and strain in cortical and cancellous bone, without substantially affecting the abutment's response. These findings emphasize that the assumption regarding bone material is not merely a technical aspect of the simulation but determines the interpretation of load transfer at the bone–implant interface, consistent with previous studies showing differences in stress distribution when bone is modeled as anisotropic versus isotropic (Geraldes & Phillips, 2014).

Cortical bone exhibits the highest sensitivity to orthotropic modeling. Principal stresses increase under all load and contact combinations, whereas stresses in cancellous bone decrease. This pattern is more accurately interpreted as a redistribution of load from cancellous to cortical bone, given the stiffness and direction-dependent mechanical behavior of cortical bone. This is consistent with the biomechanical principle that the mandibular bone is direction-dependent and that isotropic models may underestimate local stress gradients, particularly in the crestal cortical region (Lettry et al., 2003; Ün & Çalık, 2016).

The effect of the material is more limited to the abutment and screw, but the fixture exhibits a complex response. Under axial loading, the orthotropic model produces moderate stress changes, whereas oblique loading significantly reduces fixture stress compared to the isotropic model. This indicates that the effect of the material model depends on the direction of loading; thus, the orthotropic model does not universally increase biomechanical risk, but rather alters the load transfer pathway in the implant–bone system.

The strain and displacement results support this interpretation. Orthotropic modeling does not yield uniform increases or decreases; the response varies with load direction and contact conditions. Some large percentage changes are primarily due to very small isotropic baseline values, so it is relatively more accurate to present absolute magnitudes alongside percentages to avoid overstatement.

Overall, an orthotropic model is more representative for evaluating peri-implant bone response and provides greater biomechanical realism (Falcinelli et al., 2023). Isotropic models remain useful as comparative reference models, but they may obscure direction-dependent stress and strain patterns (Di Stefano et al., 2021). These findings underscore that the choice of bone material model must be explicitly justified in dental implant FEA studies, particularly when conclusions are drawn from peri-implant stress and strain distributions.

The implant–bone contact conditions clearly influence the distribution of stress, strain, and displacement in the implant–bone system. Compared to the fully bonded model, frictional contact tends to increase the von Mises stress in the metal components, particularly the fixture and screw. In isotropic bone under axial loading, for example, von Mises stress in the fixture increases by approximately 66.3%, while in the screw it increases by approximately 11%. This pattern indicates that a contact representation allowing micro-movement at the interface can alter the load transfer path, shifting some mechanical stress to the prosthetic components, particularly in areas directly involved in implant stability (Wazen et al., 2013).

The bone tissue response exhibits a more complex pattern compared to the metal component. In the isotropic axial model, frictional contact significantly increases stress and strain in the cortical bone, with $\sigma Ct$ rising from 0.24 MPa to 3.26 MPa and cortical strain increasing by approximately 409.8%. This indicates that cortical bone, as the stiffer peri-implant tissue, remains the primary area bearing the load concentration when contact conditions are not perfectly integrated (Yang et al., 2023). Conversely, changes in cancellous bone appear more moderate, suggesting that the effects of frictional contact on bone tissue are not uniform but depend on the mechanical characteristics of each bone structure.

In the orthotropic model, the effect of changing the contact from bonded to frictional becomes more heterogeneous. Although the fixture and screw still exhibit increased stress, some parameters in the cortical and cancellous bone actually decrease, particularly under oblique loading. The very large relative changes in $\varepsilon Cn$, including decreases of up to -97.4%, must be interpreted with caution because they may be influenced by very small baseline values or by changes in the direction of the strain response. Thus, these results should not be interpreted merely as simple increases or decreases, but rather as an indication that bone anisotropy can modify load transfer pathways in a direction-specific manner when the interface is modeled as frictional.

Changes in displacement further support the influence of material modeling, contact conditions, and loading direction. In the isotropic model under axial loading, frictional contact increased screw and abutment displacements by 103.4% and 129.4%, respectively, while fixture displacement increased only slightly by 10.3%. Conversely, under oblique loading, frictional contact reduced displacement in the fixture, screw, abutment, and cortical bone, whereas displacement in the cancellous bone showed a slight increase. In the orthotropic-frictional model under oblique loading, most components exhibited reduced displacement compared with bonded contact. These findings indicate that frictional contact does not uniformly increase mechanical responses but instead modifies load transfer, depending on the interaction among bone material, contact conditions, and loading direction.

Overall, these results confirm that the choice of contact conditions is a critical methodological aspect in dental implant FEA. Fully bonded contact can simplify the model by assuming perfect integration between the implant and bone, but it may limit the representation of micro-movements at the interface. Conversely, frictional contact provides a more flexible representation of bone–implant mechanical interactions, yet yields a more complex stress–strain distribution that is highly influenced by bone material and load direction (Falcinelli et al., 2023). Therefore, the rationale for contact selection must be explicitly stated to ensure that biomechanical predictions do not result in overestimation or underestimation of mechanical risks to prosthetic components or peri-implant tissues.

The direction of loading significantly influences the biomechanical response of the implant–bone system, but this influence is not uniform across all components, material models, or contact conditions. A shift from axial to oblique loading not only increases the lateral load component but also enhances the bending and shear characteristics of the system (Mie et al., n.d.). Consequently, the distribution of stress, strain, and displacement becomes more dependent on the interaction between the bone material model and the interface conditions.

Based on the data patterns, the effects of oblique load are most pronounced in the fixture, cancellous bone, and system deformation, whereas the abutment exhibits a relatively stable response.

In the isotropic model, oblique loading tends to substantially increase the mechanical response of the fixture and cancellous bone. Under isotropic–bonded conditions, the von Mises stress of the fixture increases from 45.8 MPa to 457.05 MPa, or approximately tenfold. Under isotropic–frictional conditions, an increase is also observed, from 76.161 MPa to 503.12 MPa. This pattern indicates that when bone is modeled as an isotropic material, oblique loads result in stronger mechanical concentrations at the fixture. Biomechanically, this can be explained by the increased bending moment when the force direction is no longer parallel to the implant axis, thereby increasing the transfer of lateral load to the peri-implant tissue (Sugiura et al., 2017).

The response of cancellous bone in the isotropic model also showed a clear increase, particularly under bonded conditions. The stress in cancellous bone increased from 6.3122 MPa to 88.099 MPa in the isotropic–bonded case and from 9.7093 MPa to 82.938 MPa in the isotropic–frictional case. In contrast, the response of cortical bone was not entirely linear. In bonded contact, an oblique load increases cortical bone stress, whereas in frictional contact, cortical bone stress actually decreases. These findings indicate that the effect of loading direction cannot be understood separately from the contact assumption. At a fully bonded interface, an oblique load is transmitted more directly to the cortical bone. In contrast, in frictional contact, load redistribution likely occurs, altering the stress-transfer path between cortical and cancellous bone.

In the orthotropic model, the effect of oblique loading becomes more complex. Under bonded conditions, oblique loading reduces stress in the fixture and cortical bone, but still increases stress in the cancellous bone as well as displacement in nearly all components. Conversely, under orthotropic–frictional conditions, most stress, strain, and displacement parameters tend to decrease, except for certain responses such as stress in the cancellous bone and the abutment. This pattern indicates that the direction-dependent properties of orthotropic bone significantly alter the load-transfer path. Thus, an oblique load does not always increase the absolute stress but can alter the load distribution, depending on the direction of material stiffness and the interface contact characteristics.

The screw exhibited a different pattern compared to the fixture. Across all material and contact combinations, the transition from axial to oblique loading actually reduced the screw's stress and strain. This finding reinforces the notion that oblique loading cannot be reduced to a single factor that consistently increases all mechanical parameters. Rather, oblique loading is more accurately understood as a factor that alters the load transfer path between components within the implant–prosthetic system. Meanwhile, the abutment exhibits the most stable response, with relatively small changes in stress across all scenarios. This indicates that biomechanical risks arising from changes in load direction are more pronounced in the fixture and peri-implant bone tissue than in the abutment.

The displacement parameter underscores the importance of loading direction in assessing the system's deformation response. In the isotropic–bonded case, the displacement of the cancellous bone increased from 1.08 μm to 21.65 μm, while the displacement of the fixture increased from 1.07 μm to 5.51 μm. In the orthotropic–bonded case, the increase in displacement was more pronounced across nearly all components, including the fixture, screw, abutment, cortical bone, and cancellous bone. However, in the orthotropic–frictional model, the oblique load actually reduced displacement across all components. These findings indicate that system deformation is significantly influenced by the combination of loading direction, bone material properties, and contact conditions; therefore, the interpretation of displacement must not be divorced from the model configuration.

Overall, these results indicate that the loading direction is a critical variable in FEA simulations of dental implants. Axial loads tend to produce a more controlled response because the force acts parallel to the implant axis. In contrast, oblique loads result in a more complex biomechanical response through increased bending moments, stress redistribution, and changes in system deformation (Brune et al., 2019). However, the effects of oblique loading cannot be generalized as an increase in all parameters, as the response is highly dependent on the bone material model and contact conditions. Therefore, the interpretation of FEA results should not only directly compare axial and oblique loads but also consider the interactions between loading direction, isotropic–orthotropic assumptions, and bonded–frictional conditions at the interface.

**CONCLUSION**

The results of this study indicate that the biomechanical response of the implant–bone system is influenced by the interaction between bone material modeling, implant–bone contact conditions, and loading direction, rather than by any single factor acting independently. Within the limitations of this model, cortical and cancellous bone tissue exhibit a more pronounced sensitivity to variations in material properties than the abutment. The nature of the implant–bone contact affects load-transfer mechanisms, but this effect is context-dependent. Frictional contact does not always lead to an increase in mechanical response; however, it can alter the distribution of stress and strain in both the metal components and the peri-implant tissues, depending on the combination of simulation parameters. The direction of loading plays a crucial role in determining the distribution of biomechanical responses. Axial loads tend to produce more controlled mechanical patterns, whereas oblique loads introduce bending and shear components that can alter the distribution of stress, strain, and displacement in the fixture, screw, abutment, cortical bone, and cancellous bone. In practical terms, these findings underscore the importance of simultaneously selecting material models, defining interfaces, and varying loading directions in FEA of dental implants. The resulting implications should be understood as simulation-based biomechanical guidance to support the interpretation of implant and prosthetic designs, rather than as direct clinical recommendations.

**REFERENCE**


Alemayehu, D. B., & Todoh, M. (2024). *Nonlinear Finite Element Analysis of Bone – Implant Contact in Three Short Dental Implant Models with Varying Osseointegration Percentages*. 505–524.

Alqahtani, A. R., Desai, S. R., Patel, J. R., Alqhtani, N. R., & Alqahtani, A. S. (2023). Investigating the impact of diameters and thread designs on the Biomechanics of short implants placed in D4 bone : a 3D finite element analysis. *BMC Oral Health*, 1–18. https://doi.org/10.1186/s12903-023-03370-8

Azhdari, M., Kamrava, M., Rezazadeh, G., Pathak, R., & Schulze-sp, U. (2026). *From mechanical models to clinical reality : A systematic review of finite element advances in dental implant design , biomechanics , and optimization*. *50*(September 2025). https://doi.org/10.1016/j.mtcomm.2025.114314

Brune, A., Stiesch, M., Eisenburger, M., & Greuling, A. (2019). Materials Science & Engineering C The e ff ect of di ff erent occlusal contact situations on peri-implant bone stress – A contact fi nite element analysis of indirect axial loading. *Materials Science & Engineering C*, *99*(June 2018), 367–373. https://doi.org/10.1016/j.msec.2019.01.104

Dhatrak, Pankaj, Kurup, Alekh, & Khasnis, Neha. (2023). Influence of surface coatings on the stress distribution by varying friction contact at implant-bone interface using finite element analysis. *Proceedings of the Institution of Mechanical Engineers, Part H: Journal of Engineering in Medicine*, *237*(2), 233–242. https://doi.org/10.1177/09544119221146617

Di Stefano, D. A., Arosio, P., Capparè, P., Barbon, S., & Gherlone, E. F. (2021). Stability of dental implants and thickness of cortical bone: Clinical research and future perspectives. a systematic review. In *Materials* (Vol. 14, Issue 23). https://doi.org/10.3390/ma14237183

Ding, X., Liao, S.-H., Zhu, X.-H., & Wang, H.-M. (2014). Influence of orthotropy on biomechanics of peri-implant bone in complete mandible model with full dentition. *BioMed Research International*, *2014*, 709398. https://doi.org/10.1155/2014/709398

Falcinelli, C., Valente, F., Vasta, M., & Traini, T. (2023). Finite element analysis in implant dentistry: State of the art and future directions. *Dental Materials*, *39*(6), 539–556.https://doi.org/10.1016/j.dental.2023.04.002

Fodor, C. R., & Pałka, Ł. (2025). *Experimental Biomechanical Analysis of the Bone-to-Implant Connection in Single-Piece Implants*. 1–20.

Geraldes, D. M., & Phillips, A. T. M. (2014). *A comparative study of orthotropic and isotropic bone adaptation in the femur*. *April*, 873–889. https://doi.org/10.1002/cnm

Han, J., Sun, Y., & Wang, C. (2016). *Effect of Integration Patterns Around Implant Neck on Stress Distribution in Peri-Implant Bone : A Finite Element Analysis*. *00*, 1–10. https://doi.org/10.1111/jopr.12434

Has, L. C. (2025). *Effect of bone quality, implant* *length, and loading timing on stress transmission in the posterior mandible : A Finite Element Analysis*. 1–33.

Hosseini-faradonbeh, S. A., & Katoozian, H. R. (2022). *Biomechanical evaluations of the long-term stability of dental implant using finite element modeling method : a systematic review*.

Kamal, M. N. M., Mohammed, H. A., & Shokry, A. (2025). Finite element analysis of stress distribution in unilateral distal extension partial dentures: a comparison of four attachment designs. In *BMC Oral Health* (Vol. 25, Issue 1). https://doi.org/10.1186/s12903-025-06213-w

Kriswanto, K., Bayuseno A. P., Setiawan, F., & Fitriyana, D. F. (2025). *Stress and Displacement Simulation of the Posterior Dental Implants on Variations of Applied Materials and Temperatures*. *1*(1), 164–179.

Kriswanto, K., Jamari, J., Andika, R., Bayuseno, A. P., Yusuf, A. A., & Ammarullah, M. I. (2026). *Fixture design effects on posterior dental implant stability using finite element analysis ( FEA ): a systematic review*.

Le, A. Z., Arroyo, L., Castro, G., & Health, T. (2016). *MECHANICAL CHARACTERIZATION OF BONE ALLOGRAFTS , ENRICHED WITH MESENCHYMAL CELLS*. *11*(4), 722–730. https://doi.org/10.2495/DNE-V11-N4-722-730

Lettry, S., Seedhom, B. B., Berry, E., & Cuppone, M. (2003). *Quality assessment of the cortical bone of the human mandible*. *32*, 35–44. https://doi.org/10.1016/S8756-3282(02)00921-3

Lin, P.-J., & Su, K.-C. (2020). Biomechanical Design Application on the Effect of Different Occlusion Conditions on Dental Implants with Different Positions—A Finite Element Analysis. In *Applied Sciences* (Vol. 10, Issue 17, p. 5826). https://doi.org/10.3390/app10175826

Luo, X., Rong, Q., Luan, Q., & Yu, X. (2022). Effect of partial restorative treatment on stress distributions in non - carious cervical lesions : a three - dimensional finite element analysis. *BMC Oral Health*, 1–14. https://doi.org/10.1186/s12903-022-02647-8

MatWeb, A. A. S. M. I. /. (2026). *Titanium Ti-6Al-4V (Grade 5), Annealed – Material Property Data*. MatWeb / ASM Aerospace Specification Metals Inc. https://www.matweb.com/search/datasheet.aspx?MatGUID=a0655d261898456b958e5f825ae85390&utm.com

Mie, J., Koyama, F., Dayrell, A. C., Leonardo, R., Consani, X., Elias, G., Henriques, P., & Mesquita, M. F. (n.d.). *Stress Evaluation of Implant-Abutment Connections Under Different Loading Conditions : A 3D Finite Element Study*. 133–137. https://doi.org/10.1563/AAID-JOI-D-11-00205

Nakamura, F., Jinno, Y., Yamasaki, Y., Furuta, M., Takeshita, T., Sakamoto, Y., Nakamura, T., & Ayukawa, Y. (2025). The Impact of Posterior Occlusal Support Recovery by Dental Implant Treatment on the Survival of Remaining Teeth: A Long-Term Retrospective Study. In *Journal of Clinical Medicine* (Vol. 14, Issue 24, p. 8939). https://doi.org/10.3390/jcm14248939

Niroomand, M. R., & Arabbeiki, M. (2020). Informatics in Medicine Unlocked Implant stability in different implantation stages : Analysis of various interface conditions. *Informatics in Medicine Unlocked*, *19*, 100317. https://doi.org/10.1016/j.imu.2020.100317

Park, J., Park, S., Kang, I., & Noh, G. (2022). Biomechanical effects of bone quality and design features in dental implants in long-term bone stability. *Journal of Computational Design and Engineering*, *9*(5), 1538–1548. https://doi.org/10.1093/jcde/qwac069

Prados-privado, M., Mart, C., Gehrke, S. A., & Prados-frutos, J. C. (2020). *Influence of Bone Definition and Finite Element Parameters in Bone and Dental Implants Stress :*

Prados-Privado, M., Martínez-Martínez, C., Gehrke, S. A., & Prados-Frutos, J. C. (2020). Influence of Bone Definition and Finite Element Parameters in Bone and Dental Implants Stress: A Literature Review. In *Biology* (Vol. 9, Issue 8, p. 224). https://doi.org/10.3390/biology9080224

Qiu, P., Cao, R., Li, Z., & Fan, Z. (2024). Heliyon Review article A comprehensive biomechanical evaluation of length and diameter of dental implants using finite element analyses : A systematic review. *Heliyon*, *10*(5), e26876. https://doi.org/10.1016/j.heliyon.2024.e26876

Sugiura, T., Yamamoto, K., & Horita, S. (2017). *Effects of implant tilting and the loading direction on the displacement and micromotion of immediately loaded implants : an in vitro experiment and finite element analysis*. *47*(4), 251–262.

Taheri, R. A., Jarrahi, A., Farnoosh, G., & Karimi, A. (2018). A comparative finite element simulation of stress in dental implant–bone interface using isotropic and orthotropic material models in three mastication cycles. *Journal of the Brazilian Society of Mechanical Sciences and Engineering*, *40*(10), 489. https://doi.org/10.1007/s40430-018-1409-9

Ün, K., & Çalık, A. (2016). *Relevance of inhomogeneous – anisotropic models of human cortical bone : a tibia study using the finite element method*. *2818*(March). https://doi.org/10.1080/13102818.2016.1154803

Wazen, R. M., Currey, J. A., Guo, H., Brunski, J. B., Helms, J. A., & Nanci, A. (2013). Acta Biomaterialia Micromotion-induced strain fields influence early stages of repair at bone – implant interfaces. *Acta Biomaterialia*, *9*(5), 6663–6674. https://doi.org/10.1016/j.actbio.2013.01.014

Yang, Y., Liu, Y., Yuan, X., Ren, M., Chen, X., Luo, L., Zheng, L., & Liu, Y. (2023). Three-dimensional finite element analysis of stress distribution on short implants with different bone conditions and osseointegration rates. In *BMC Oral Health* (Vol. 23, Issue 1). https://doi.org/10.1186/s12903-023-02945-9

Yorioka, H., Otsu, Y., Suzuki, R., Matsunaga, S., Nakano, T., Abe, S., & Sasaki, H. (2024). The influence of immediate occlusal loading on micro/nano-structure of peri-implant jaw bone in rats. *International Journal of Implant Dentistry*, *10*(1), 24. https://doi.org/10.1186/s40729-024-00538-x